

On the Electronic Structure of Mesitylnickel Complexes of α -Diimines — Combining Structural Data, Spectroscopy and Calculations

Axel Klein,^{*[a][‡]} Martin P. Feth,^{*[b]} Helmut Bertagnolli,^[b] and Stanislav Zális^[c]

Keywords: Density functional calculations / Electronic structure / EXAFS / Nickel / Raman spectroscopy

New organometallic nickel complexes of the type [(α -diimine)-Ni(Mes)Br] and [(α -diimine)Ni(Mes)₂] (Mes = mesityl = 2,4,6-trimethylphenyl) were prepared and characterised spectroscopically in detail. A combination of spectroscopic techniques (XRD, EXAFS, absorption, resonance Raman) and quantum chemical (DFT) calculations reveals the interplay of the diimine ligands and the mesityl or bromine co-

ligands with the nickel centre. The low-lying electronic transitions are assigned as mixed MLCT/L'LCT or MLCT/XLCT due to low-lying accepting π^* -orbitals centred on the diimine ligands and mixed metal/co-ligand MOs as donor levels.

(© Wiley-VCH Verlag GmbH & Co. KGaA, 69451 Weinheim, Germany, 2004)

Introduction

Organometallic nickel complexes with α -diimine ligands like 2,2'-bipyridine (bpy), 1,10-phenanthroline (phen) or diazabutadienes (R-DAB) have gained an enormous interest in the last decade. This is mainly due to their success as effective catalysts in olefin polymerisation or olefin/CO copolymerisation.^[1–9] It has been established, mainly by Brookhart, that methylnickel complexes with carefully designed diazabutadiene ligands exhibit higher activities than the classical Ziegler catalysts combined with a greatly reduced sensibility towards poisoning by polar functions. Detailed investigations on the activities of various derivatives on polymerisation,^[1a] theoretical calculations on the mechanisms and energetics^[2] and the use of these compounds for other catalytic purposes^[10–13] have been published so far.

In the 1960s these compounds were already known as darkly coloured very reactive materials.^[14–17] Detailed

investigation of their structures and electronic properties, however, were scarce^[15,18–20] until Yamamoto et al. recently reported and discussed the optical spectra of some alkyl and aryl complexes with 2,2'-bipyridine (bpy).^[21] In this report the spectra were mainly used to monitor elimination processes. In order to fill that gap we initiated a detailed and combined research project using various spectroscopic techniques (absorption, emission and resonance Raman) and quantum chemical calculations, with a focus on the optical properties.

One reason why such investigations have not been performed so far is probably the high sensitivity of such alkyl-nickel complexes towards oxygen or moisture.^[19] They also easily undergo thermal decomposition by reductive elimination.^[21,22] Aryl derivatives are much more inert towards water or oxygen, although the threat of reductive elimination (forming biaryls) remains.^[22] We have recently shown that introducing the bulky mesityl co-ligand (Mes = 2,4,6-trimethylphenyl) results in very stable mesityl- and dimesitylnickel complexes^[23] of 2,2'-bipyridine, and, with the proper choice of ligands, compounds such as [(N[^]N)Ni(Mes)Br] (N[^]N = α -diimine) have allowed us to carry out a detailed study of the ligand-exchange behaviour of these complexes using EXAFS and spectroscopic techniques like NMR or absorption spectroscopy.^[24]

In this paper we wish to report the synthesis and detailed spectroscopic and structural (EXAFS + XRD) characterisation of a series of bromomesityl- and dimesitylnickel complexes of various diimine ligands together with the results of a detailed study of the electronic properties of selected samples using a combination of spectroscopy (absorption, resonance Raman) and quantum chemical calculations. The latter were based on the molecular structures established by single-crystal XRD measurements and EXAFS spec-

[a] Institut für Anorganische Chemie, Universität Stuttgart, Pfaffenwaldring 55, 70569 Stuttgart, Germany
Fax: +49-(0)711-685-4165

E-mail: aklein@iac.uni-stuttgart.de

[b] Institut für Physikalische Chemie, Universität Stuttgart, Pfaffenwaldring 55, 70569 Stuttgart, Germany
Fax: +49-(0)711-685-4443

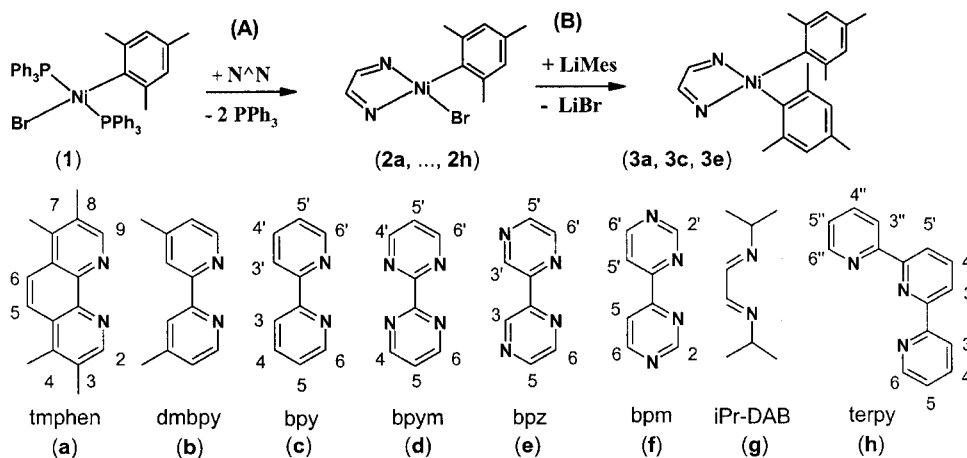
E-mail: m.feth@ipc.uni-stuttgart.de

[c] J. Heyrovský Institute of Physical Chemistry, Academy of Sciences of the Czech Republic, Dolejškova 3, 18 000 Prague 8, Czech Republic
E-mail: zalis@jh-inst.cas.cz

[‡] Present address: Institut für Chemie, Karl-Franzens-Universität Graz
Schubertstrasse 1, 8010 Graz, Austria
Fax: +43-(0)316-380-9835

E-mail: axel.klein@uni-graz.at

Supporting information for this article is available on the WWW under <http://www.eurjic.org> or from the author.



Scheme 1. Preparation of the α -diimine complexes with numbering: tmphen = 3,4,7,8-tetramethyl-1,10-phenanthroline, dmbpy = 4,4'-dimethyl-2,2'-bipyridine, bpy = 2,2'-bipyridine, bpm = 2,2'-bipyrimidine, bpz = 2,2'-bipyrazine, bpm = 4,4'-bipyrimidine, *i*Pr-DAB = *N,N'*-diisopropyl-1,2-ethanediimine (*N,N'*-diisopropyl-1,4-diazabutadiene), terpy = 2,2',6'-terpyridine

troscopy. The compounds under study are bromomesityl complexes of the type $[(N^{\wedge}N)Ni(Mes)Br]$ ($N^{\wedge}N$ = diimine ligands, Mes = mesityl = 2,4,6-trimethylphenyl) with various α -diimine ligands and, additionally, selected dimesityl complexes $[(N^{\wedge}N)Ni(Mes)_2]$ (see Scheme 1).

Results and Discussion

Synthesis and General Properties

The neutral complexes $[(N^{\wedge}N)Ni(Mes)Br]$ ($N^{\wedge}N$ = diimine ligands) were synthesised from the precursor complex $[(PPh_3)_2Ni(Mes)Br]$ (**1**) by ligand-exchange reactions in acetone or toluene solution [see Scheme 1 (A)] and were analysed by 1H and ^{13}C NMR spectroscopy and elemental analysis (see Table 1).

For rather basic diimine ligands like bpy or tmphen reaction A proceeds very smoothly with high yields. The less

basic the diimine ligands are (e.g. bpz or bpm) the more the equilibrium tends towards the starting materials. For *i*Pr-DAB the procedure had to be varied to obtain reasonable yields (see Exp. Sect.). With the very weakly basic ligand *N,N'*-di(2,6-xylyl)-1,2-ethanediimine (*Xyl*-DAB) no product was formed upon reaction with $[(PPh_3)_2Ni(Mes)Br]$ (**1**). Once formed, and in the absence of PPh_3 or other strong ligands, the compounds are stable in solvents like CH_2Cl_2 , THF, toluene or acetone towards ligand-exchange reactions.^[24] The complex $[(terpy)Ni(Mes)]Br$ (**2h**) was prepared following the same method. The 1H NMR spectroscopic data reveal that all three pyridine units bind to nickel and that Br serves only as a counteranion to the cationic complex. The dimesityl complexes $[(N^{\wedge}N)Ni(Mes)_2]$ (**3**) were prepared for selected samples by reacting the bromomesityl complexes with mesityllithium as shown in Scheme 1 (B).

The NMR spectroscopic data reflect the geometric properties of the compounds. The bromomesityl complexes

Table 1. 1H NMR spectroscopic data and details of the preparation of complexes $[(N^{\wedge}N)Ni(Mes)Br]$

	1H NMR δ (ppm) ^[a]							Yield (%)	Formula (mol. mass)	Elem. anal. found C, H, N (calcd.) (%)
2a	2,9	5,6	Me ^{4,7}	Me ^{3,8}	<i>m</i> -H	<i>o</i> -Me	<i>p</i> -Me	92	C ₂₅ H ₂₇ BrN ₂ Ni (494.11)	60.79 (60.77), 5.61 (5.51), 5.68 (5.67)
	7.09, 9.28	8.25	2.78	2.65, 2.61	6.50	3.09	2.75			
2b	6,6'	3,3'	Me ^{4,4'}	5,5'	<i>m</i> -H	<i>o</i> -Me	<i>p</i> -Me	88	C ₂₁ H ₂₃ BrN ₂ Ni (442.04)	57.13 (57.06), 5.25 (5.24), 6.35 (6.34)
	9.20, 6.98	8.18, 8.16	2.51, 2.39	7.49, 7.14	6.43	3.03	2.17			
2c	6,6'	3,3'	4,4'	5,5'	<i>m</i> -H	<i>o</i> -Me	<i>p</i> -Me	95	C ₁₉ H ₁₉ BrN ₂ Ni (413.98)	55.33 (55.12), 4.65 (4.63), 6.72 (6.77)
	9.42, 7.20	8.35, 8.31	8.18, 8.15	7.70, 7.34	6.35	3.05	2.14			
2d	6,6'	4,4'	4,4'	5,5'	<i>m</i> -H	<i>o</i> -Me	<i>p</i> -Me	75	C ₁₇ H ₁₇ BrN ₄ Ni (415.97)	49.10 (49.09), 4.09 (4.12), 13.13 (13.47)
	9.63, 7.40	9.21, 9.13	7.92, 7.58	6.47	3.02	2.19				
2e	3,3'	6,6'	5,5'	<i>m</i> -H	<i>o</i> -CH ₃	<i>p</i> -CH ₃	78	C ₁₇ H ₁₇ BrN ₄ Ni (322.73)	48.92 (49.09), 4.02 (4.12), 13.21 (13.47)	
	9.71, 9.52	9.80, 7.33	9.12, 8.75 s	6.50 s	2.91 s	2.20 s				
2f	2,2'	6,6'	5,5'	<i>m</i> -H	<i>o</i> -CH ₃	<i>p</i> -CH ₃	75	C ₁₇ H ₁₇ BrN ₄ Ni (322.73)	49.02 (49.09), 4.13 (4.12), 13.41 (13.47)	
	10.04 s, 7.85 s	8.08 d, 8.02 d	9.36 d, 9.25 d	6.51 s	2.30 s	2.21 s				
2g	H imine		H <i>Ci</i> Pr	H ₃ C <i>i</i> Pr	<i>m</i> -H	<i>o</i> -CH ₃	<i>p</i> -CH ₃	82	C ₁₇ H ₂₇ BrN ₂ Ni (398.03)	56.55 (57.07), 6.29 (6.59), 32.09 (31.60)
	8.55 s, 8.43 s		3.26 m	1.03 d	6.42	2.97 s	2.21 s			
2h	6,6'';3,3''	4,4''	5,5''	3',5';4'	<i>m</i> -H	<i>o</i> -CH ₃	<i>p</i> -CH ₃	95	C ₂₄ H ₂₆ BrN ₃ Ni (495.10)	58.73 (59.26), 6.88 (1.18), 30.59 (29.17)
	7.48 qd, 8.69 d	8.35 ddd	7.61	8.72, 8.52	6.72 s	2.96 s	2.29 s			

[a] Measured in [D₆]acetone.

give full sets of ^1H and ^{13}C resonances (see Table 1 and Supporting Information) for the chelate ligands, confirming the planar geometry and C_S symmetry. For the dimesityl complexes C_2 symmetry can be deduced from the NMR spectra.

Structures

The structures of the investigated complexes are essential for the discussion of electronic properties since the molecular entity must be unequivocal. Also, the optical spectroscopy might be affected by intermolecular interactions like stacking and, finally, they serve as a basis for the quantum chemical calculations. Selected samples were therefore submitted to single-crystal XRD or powder EXAFS study.

XRD

The crystal structures of two examples of the series $[(N^{\wedge}N)\text{Ni}(\text{Mes})\text{Br}]$ with $N^{\wedge}N = \text{bpy}$ (**2c**) or *i*Pr-DAB (**2g**)^[24] and the structure of $[(\text{bpy})\text{Ni}(\text{Mes})_2]$ (**3c**)^[23] have recently been published. In this paper we report the crystal structure of $[(\text{tmphen})\text{Ni}(\text{Mes})_2]$ (**3a**; Figure 1). The reason for adding this structure to the series is because of the special character of the tmphen ligand. In the series shown in Scheme 1 tmphen is the most basic ligand and, more importantly, it is a much more rigid ligand than bpy or the bidiazines. This has a strong impact on the molecular structure since previous studies have revealed that the steric demand of two *cis* oriented mesityl substituents in square-planar complexes of nickel, palladium or platinum leads to marked deviations not only in the coordination sphere but also within the diimine ligands.^[23–25] This rigidity also has a strong impact on the optical properties, as we will see later.

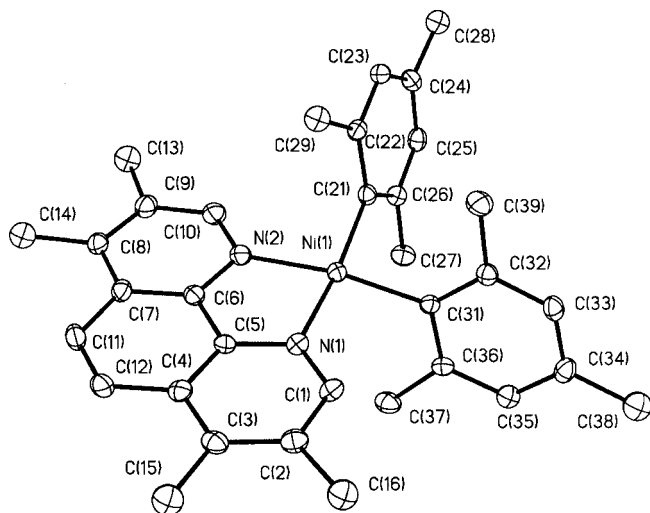


Figure 1. Molecular structure of **3a** (50% probability ellipsoids; H atoms omitted for clarity); selected bond lengths (Å) and angles (deg): Ni–N(1) 1.975(4), Ni–N(2) 1.960(4), Ni–C(11) 1.911(4), Ni–C(21) 1.914(4), N(1)–C(1) 1.337(6), N(2)–C(10) 1.333(6), N1–C(5) 1.345(13), N2–C(6) 1.385(12); N(1)–Ni–N(2) 82.55(16), C(11)–Ni–C(21) 90.47(18), N(1)–Ni–C(11) 94.01(17), N(1)–Ni–C(21) 168.30(17), N(2)–Ni–C(21) 94.79(17), N(2)–Ni–C(11) 169.65(18)

The structure was solved in the orthorhombic $Pbca$ space group (for details see Exp. Sect.). A solution in $P2_1/n$, which is the space group obtained for the bpy derivative **3c**, gave slightly worse R values. The crystal structure reveals that the complex forms dimers in the unit cell which are π -stacked in a non-graphite-like fashion, with an interplanar distance of 3.49(1) Å. As displayed in Figure 2 the two central rings overlap but are not completely eclipsed (shift of 0.69 Å). The interplanar distance is similar to that in the recently studied isoleptic complex $[(\text{tmphen})\text{Pt}(\text{Mes})_2]$,^[25d] but longer than the distance found in graphite (3.354 Å). For the platinum complex a similar distance of 3.52(1) Å was found but the ligands stack in a staggered fashion and are also not back-to-back, but offset.

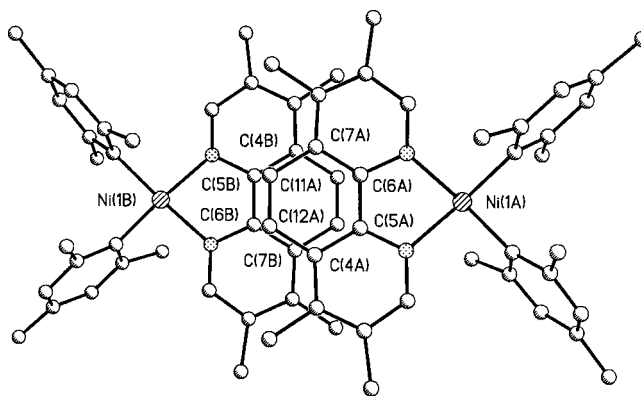


Figure 2. Stacking of two molecules of **3a** in the unit cell

The molecular structure of **3a** resembles in many respects that of the bpy derivative **3c**. The essential distances, for example Ni–N or Ni–C, and the chelate bite angle (around 82°) are very similar. The distortion of the square-planar coordination plane is higher (15.1° vs. 12.4°), as expected. In both cases the distortion of the diimine ligand is quite small (2.8° vs. 3.1°). The mesityl substituents are tilted towards the coordination plane [C(21)–N(2)–Ni(1)–N(1)–C(31)] by 70.0(6)° and 69.0(6)°, respectively, as was observed for other square-planar dimesityl complexes.^[23,25] In the related complex $[(\text{bpy})\text{Ni}(\text{C}_6\text{F}_5)_2]$ ^[22a] the C_6F_5 coligands are oriented almost perpendicular to the coordination plane and both the Ni–N distances [1.938(3) and 1.935(3) Å] and the Ni–C distances [1.903(3) and 1.907(3) Å] are markedly shorter. The N–Ni–N bite angle (82.9°) lies in the normal range whereas the C–C bond between the two pyridyl units is noticeably elongated to 1.477(7) Å. The latter is a clear indication of reduced back-bonding to the diimine ligand due to the fact that the fluoroaryl coligands donate much less electron density than their mesityl counterpart in the complexes **3a** and **3c**. This is also the reason for the different Ni–C bond lengths in the two types of arylnickel complexes. We thus conclude that the aryl coligand strongly governs the geometry around the nickel atom (and also the electron distribution).

EXAFS Spectroscopy

In the Ni-K edge XANES spectra of all complexes the typical two pre-edge peaks of square-planar Ni^{II} complexes can be observed.^[26] The pre-peak at about 8333 eV can be assigned to a 1s→3d electron transition, while the second peak, which occurs at about 8337 eV, is due to a 1s→4p_z transition with shakedown contributions.^[26a]

The obtained structural parameters of the investigated complexes determined by curve fitting analysis of the EXAFS spectra at the Ni-K and Br-K edge are summarised in Table 2. [(dmbpy)Ni(Mes)Br] (**2b**), [(bpym)Ni(Mes)Br] (**2d**) and [(bpz)Ni(Mes)Br] (**2e**) show very similar EXAFS functions at the Ni-K and Br-K edge, leading to almost identical structural parameters, which are in very good agreement with values found from single crystal XRD and from the EXAFS analysis of the complex [(bpy)Ni(Mes)Br] (**2c**).^[24] As an example, Figure 3 shows the k³-weighted EXAFS spectra coupled with the magnitudes of the Fourier transforms of **2e** at the Ni-K (a and b) and at the Br-K edge (c and d) The fitting of the Ni-K edge EXAFS spectra was performed using a three-shell model in which the first coordination shell at about 1.9 Å consists of the two coordinating nitrogen atoms of the diimine ligand and the carbon atom of the mesityl group, the second shell contains the

bromine backscatterer at about 2.3 Å and the third coordination shell at about 2.8 Å contains the further backbone-carbon atoms of the mesityl and diimine ligand. Because of the quite equal distances and backscatter behaviour of the nitrogen and carbon backscatterers in the first coordination shell, only one shell was fitted with nitrogen amplitude- and phase-functions. The Br-K edge EXAFS spectra were fitted with one coordination shell of nickel at about 2.3 Å. In complex **2a** a slightly higher Ni–C/N distance (1.97 Å) of the first coordination shell was detected, although the Ni–Br distance is of the same order of magnitude.

In Figure 4 (a) a comparison of the experimental k³-weighted EXAFS functions of [(tmphen)Ni(Mes)₂] (**3a**), [(bpy)Ni(Mes)₂] (**3c**) and [(bpz)Ni(Mes)₂] (**3e**) at the Ni-K edge is shown. The spectra of **3a**, **2h**, **3c** and **3e** were fitted with a two-shell model: the first shell is due to the carbon and nitrogen atoms of the imine and mesityl ligands coordinating directly to the nickel centre atom and the second shell consist of the backbone carbon atoms of the ligands. The structural parameters of **3a**, **2h** and **3c** determined by EXAFS are very similar.

At first sight the complex [(bpz)Ni(Mes)₂] (**3e**) seems to deviate from **3a**, **2h** and **3c**. The peak of the first coordination shell in the Fourier-transformed EXAFS spectrum

Table 2. Structural parameters of the solid complexes determined from the Ni-K and Br-K edge EXAFS spectrum

[(N [^] N)Ni(Mes)Br] N [^] N	[a]	r (Å)	N	σ [Å]	ΔE ₀ (eV)	k-range (Å ⁻¹)	Fit-Index
tmphen (2a)	Ni–C/N	1.97 ± 0.02	2.6 ± 0.3	0.108 ± 0.009	22.3	3.90–13.90	37.3
	Ni–Br	2.30 ± 0.02	0.8 ± 0.1	0.071 ± 0.011			
	Ni–C	2.82 ± 0.03	1.9 ± 1.4	0.089 ± 0.027			
	Br–Ni	2.30 ± 0.02	0.9 ± 0.1	0.063 ± 0.006			
dmbpy (2b)	Ni–C/N	1.93 ± 0.02	3.1 ± 0.3	0.093 ± 0.006	13.8 25.6	4.00–13.10 3.70–13.00	41.0 27.6
	Ni–Br	2.29 ± 0.02	0.9 ± 0.2	0.062 ± 0.008			
	Ni–C	2.79 ± 0.03	3.8 ± 1.1	0.099 ± 0.019			
	Br–Ni	2.29 ± 0.02	1.0 ± 0.1	0.064 ± 0.007			
bpy ^[24] (2c)	Ni–C/N	1.92 ± 0.02	3.1 ± 0.3	0.081 ± 0.008	18.5 28.0	4.40–13.40 3.60–14.90	47.8 21.8
	Ni–Br	2.30 ± 0.02	1.0 ± 0.2	0.062 ± 0.011			
	Ni–C	2.81 ± 0.03	5.6 ± 1.7	0.110 ± 0.030			
	Br–Ni	2.30 ± 0.02	0.9 ± 0.1	0.060 ± 0.006			
bpym (2d)	Ni–C/N	1.91 ± 0.02	2.8 ± 0.3	0.056 ± 0.006	14.5 27.6	3.60–11.30 3.70–12.50	23.5 23.7
	Ni–Br	2.29 ± 0.02	1.2 ± 0.2	0.054 ± 0.008			
	Ni–C	2.82 ± 0.03	2.8 ± 0.8	0.063 ± 0.019			
	Br–Ni	2.29 ± 0.02	0.9 ± 0.1	0.051 ± 0.007			
bpz (2e)	Ni–C/N	1.92 ± 0.02	3.3 ± 0.3	0.093 ± 0.009	13.5 25.1	4.00–12.50 3.70–15.00	30.6 25.5
	Ni–Br	2.29 ± 0.02	0.8 ± 0.1	0.058 ± 0.008			
	Ni–C	2.80 ± 0.03	4.6 ± 1.4	0.090 ± 0.027			
	Br–Ni	2.29 ± 0.02	1.0 ± 0.1	0.064 ± 0.006			
[(terpy)Ni(Mes)]Br (2h)	Ni–C/N	1.89 ± 0.02	3.6 ± 0.4	0.075 ± 0.008	16.5 25.6	3.70–14.00 3.80–14.00	30.6 29.9
	Ni–C	2.79 ± 0.03	4.0 ± 1.2	0.060 ± 0.018			
[(N [^] N)Ni(Mes) ₂] tmphen (3a)	Ni–C/N	1.91 ± 0.02	3.5 ± 0.4	0.083 ± 0.008	29.5	3.80–11.90	36.7
	Ni–C	2.81 ± 0.03	3.6 ± 1.1	0.095 ± 0.029			
bpy (3c)	Ni–C/N	1.94 ± 0.02	3.7 ± 0.4	0.087 ± 0.009	28.9	3.80–11.50	32.7
	Ni–C	2.85 ± 0.03	5.3 ± 1.6	0.111 ± 0.033			
bpz (3e)	Ni–C/N	2.01 ± 0.02	4.4 ± 0.4	0.104 ± 0.009	21.8	3.40–11.00	36.2
	Ni–C	2.90 ± 0.03	4.3 ± 1.6	0.107 ± 0.033			

[a] Absorber–backscatterer distance r, coordination number N, Debye–Waller factor σ, with their calculated deviations, shift of the threshold energy ΔE₀ and the fit-index R.

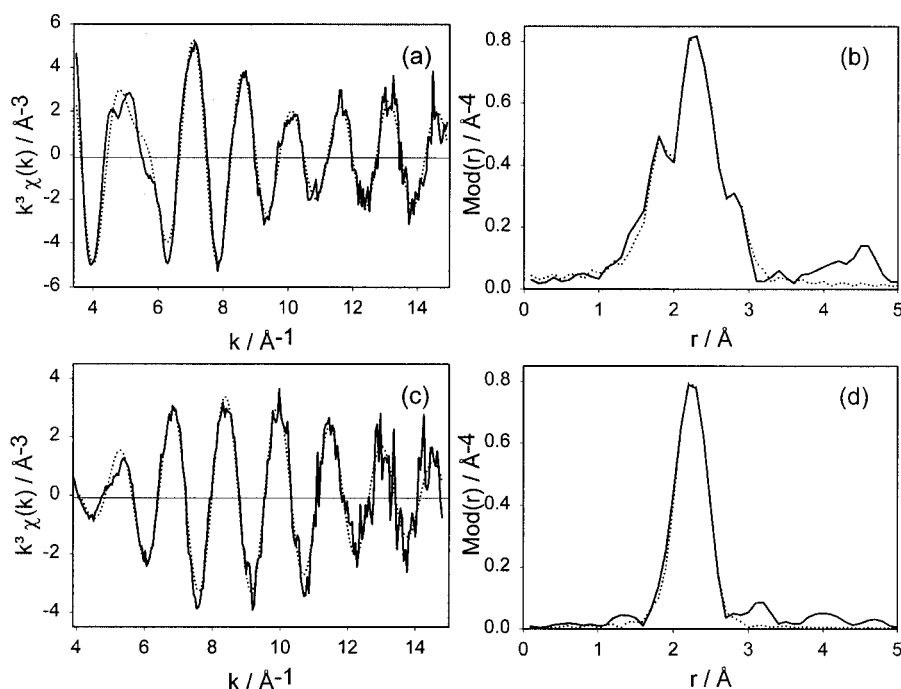


Figure 3. Experimental (solid line) and calculated (dotted line) $k^3\chi(k)$ functions (a,c) and their Fourier transforms (b,d) of solid [(bpz)Ni(Mes)Br] (**2e**) at the Ni-K (a,b) and Br-K edge (c,d)

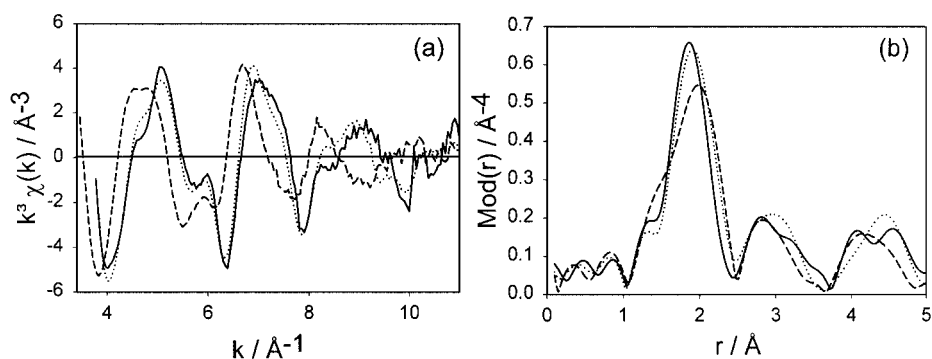


Figure 4. Comparison of the experimental $k^3\chi(k)$ functions (a) and their Fourier transforms (b) of solid [(tmphen)Ni(Mes)₂] (**3a**) (solid line), solid [(bpy)Ni(Mes)₂] (**3c**) (dotted line) and solid [(bpz)Ni(Mes)₂] (**3e**) (dashed line) (Ni-K edge)

of **3e** shows a clear asymmetry, indicating longer and shorter bonded backscatterers in the local environment of the Ni central atoms. However, a fit of two separate coordination shells did not lead to a satisfying result, thus only one coordination shell for the direct environment of nickel was fitted. The determined Ni–C/N distance of 2.01 Å for this shell is significantly longer than in the other dimesityl complexes, such as in [(bpy)Ni(Mes)₂] (**3c**) (Ni–C/N distance of 1.94 Å). Comparing the bpy complex with the tmphen derivative reveals slightly longer averaged distances for the former. In this series of ligands tmphen represents the high-basicity end and bpy is therefore less basic. Bpz is a much better π -acceptor but therefore a much weaker base,

and this gives rise to the lengthening of the Ni–N bonds. The consequences of the basicity of the various ligands for the preparation of the complexes has already been discussed. For the bromomesityl complexes this trend is reversed — the longest average distances are found for the tmphen derivative. This can be explained in the following way. Assuming that the Ni–C and Ni–N bond *trans* to Mes are essentially the same as for the dimesityl complexes, and that the Ni–Br distances are more or less constant, the length of the Ni–N bond *trans* to Br must be the reason for the observed trend. Br is a π -donor which is best accommodated by a good π -acceptor diimine ligand and tmphen in that sense is the worst in our series, whereas bpy is the best.

Optical Spectroscopy and Calculations

Absorption Spectroscopy and Calculations

Both dimesityl and bromomesityl nickel complexes are brightly coloured, ranging from orange to green in the solid as well as in solution. The absorption spectra (see Figure 5) are dominated by two broad bands of medium intensity in the visible region and an intense band in the UV region. Additional weak, very-long-wavelength bands appear as shoulders in the near IR (NIR) region which, in most cases, are only clearly visible in apolar solvents (Table 3). The two broad bands show a strong negative solvatochromism (see for example Table 4–7) they are red-shifted for the dimesityl complexes relative to their bromomesityl analogues, and in apolar solvents they are partly structured. The UV band is solvent invariant and appears to be characteristic of the ligand.

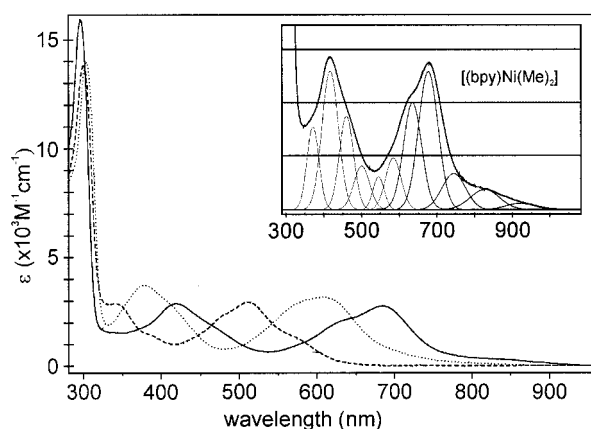


Figure 5. Absorption spectra of [(bpy)Ni(Me)₂] (solid line), [(bpy)Ni(Mes)₂] (dotted line) and [(bpy)Ni(Mes)Br] (dashed) in toluene solution; the insert depicts the spectral deconvolution for [(bpy)Ni(Me)₂].

In agreement with recent work by Yamamoto^[21] we can assign the two long-wavelength bands to charge-transfer transitions (CT) to the π^* orbitals of the diimine ligands and the UV bands to ligand-centred π - π^* transitions. In view of the observed solvatochromism of the extremely long-wavelength bands an assignment of these bands to metal-centred (LF) transitions is unlikely.

A closer look at the solvatochromism data (Table 4) reveals that the extent, as derived from the differences of the observed maxima in pentane and DMF solution, increases with the absolute energy, which parallels the series of increasing basicity (or decreasing π -acceptor character; Table 3). Generally the bromomesityl complexes exhibit stronger solvatochromism than the dimesityl derivatives and there is no marked difference between the dimethyl complex [(bpy)Ni(Me)₂] and its mesityl analogue. Extreme values are found for **2a**, underlining the special character of the tmphen ligand mentioned above, and for **3e**. All these findings are in full agreement with the simple model of a more or less strong polarisation $M^{(\delta^-)} \leftarrow L^{(\delta^+)}$ in the ground state, which is transformed to a rather apolar $M \leftarrow L$ excited state by an MLCT excitation.^[28] Strongly basic ligands favour more pronounced polarisation, whereas the donating Mes co-ligands prevent the negative polarisation of the metal by the diimine ligand.

Recently we have discussed the occurrence of mixed MLCT/L'LCT (ligand-to-ligand charge transfer) transitions (instead of pure MLCT transitions) due to contributions of the co-ligands to the frontier orbitals in related diarylplatinum complexes.^[29] To probe for such contributions from the mesityl or the bromine co-ligands we have examined the dimesitylnickel complex, the dimethylnickel complex and the bromo(mesityl)nickel complex of 2,2'-bipyridine in a combined spectroscopic and quantum chemical study.

First of all the molecular structures were calculated by both ADF/BP and G03/B3LYP methods. Both methods re-

Table 3. Absorption maxima of the nickel complexes in toluene

[(N [^] N)Ni(Mes)Br] (N [^] N)	λ (ϵ in 1000 M ⁻¹ ·cm ⁻¹) ^[a]				
	λ_1	λ_2	λ_3	λ_4	λ_5
tmphen (2a)	300	327, 343	430 sh, 452	485	527 sh
terpy (2h)		341, 365 sh	427, 453	487	531 sh
dmbpy (2b)		344	456 sh, 486 sh	507	555 sh
bpy (2c)	300	342 (2.95)	448 sh, 483 sh	516 (3.01)	571 (1.71)
bpym (2d)	293	352 sh	490 sh, 507 sh	528	592 sh
bpz (2e)	329	368 sh	402 sh, 475	564, 653 sh	790
<i>i</i> Pr-DAB (2g)	–	361	427	559 sh, 590	729 sh
bpm (2f)	–	356, 401 sh	538 sh, 610 sh	632, 650 sh	697 sh, 728 sh
[(N [^] N)NiMes ₂] (N [^] N)					
tmphen (3a)	297sh	355, 378 sh	505 sh, 543,	564	
bpy (3c)	307 (14.0)	377 (3.26)	531 sh, 587 sh	611 (3.11)	710 sh, 785 sh
bpz (3e)	333	408	462 sh, 628 sh	662	
[(bpy)NiMe ₂]	294 (15.9)	416 (2.81)	582 sh, 631 sh	678 (2.75)	785 sh, 870 sh

^[a] Absorption maxima, λ , in nm; main maxima are in italics.

Table 4. Long-wavelength absorption bands of selected nickel complexes in various solvents — solvatochromism^[a]

[(N [^] N)Ni(Mes)Br] (N [^] N)	λ (in nm)		$\tilde{\nu}$ (in cm ⁻¹)		Δ (cm ⁻¹) ^[c]
	pentane ($E^* = 0$) ^[b]	THF (0.59)	CH ₂ Cl ₂ (0.67)	DMF (0.95)	
tmphen (2a)	518 (19300)	469 (21310)	423 (23630)	409 (24435)	5135
bpy (2c)	558 (17930)	500 (20000)	490 (20410)	464 (21530)	3600
bpz (2e)	594 (16850)	545 (18360)	547 (18270)	526 (19030)	2180
<i>i</i> Pr-DAB (2g)	615 (16250)	572 (17490)	569 (17580)	547 (18270)	2020
[(terpy)Ni(Mes)] ⁺	494 (20240)	450 (22220)	460 (21760)	453 (22090)	1850
[(N [^] N)Ni(Mes) ₂] (N [^] N)	pentane	THF	CH ₂ Cl ₂	DMF	Δ (cm ⁻¹) ^[c]
tmphen (3a)	598 (16720)	546 (18330)	531 (18830)	522 (19160)	2440
bpy (3c)	645 (15500)	584 (17120)	576 (17350)	560 (17860)	2360
bpz (3e)	681 (14670)	642 (15580)	636 (15720)	629 (15890)	1220
[(bpy)Ni(Me) ₂]	toluene (0.30)	THF	CH ₂ Cl ₂	DMF	Δ (cm ⁻¹) ^[c]
[(bpy)Ni(Mes) ₂]	683 (14640)	—	—	615 (16250)	1610
[(bpy)Ni(Mes)Br]	608 (16450)	584 (17120)	576 (17350)	560 (17860)	1445
[(bpy)Ni(Mes)Br]	516 (19380)	500 (20000)	490 (20410)	464 (21530)	2150

^[a] Absorption maxima, λ , in nm; wavenumbers (in cm⁻¹) in parentheses. ^[b] E^* values are Manuta and Lees' solvent parameters for charge-transfer transitions.^[27] ^[c] $\Delta = E_{(\text{dmf})} - E_{(\text{pentane})}$, or $E_{(\text{toluene})}$ in cm⁻¹. A complete table is provided with the Supporting Information.

Table 5. Selected calculated lowest TD DFT singlet excitation energies for [(bpy)Ni(Mes)₂]

Main character (%)	ADF/SAOP		Experiment	
	Trans. energy in eV (nm)	Osc. strength	λ (nm) in toluene (ϵ) ^[a]	λ (nm) in DMF ^[a]
¹ A 95 (58b → 59b)	1.57 (790)	0.004	789 (200)	745
¹ A 38 (57b → 59b); 37 (56b → 59b); 10 (58b → 60b)	2.18 (568)	0.026	611 (2610)	554
¹ A 88 (58b → 60b); 3 (57b → 59b)	2.34 (530)	0.005	575 (1990)	535
¹ B 87 (58b → 63a); 8 (60a → 60b)	2.54 (488)	0.004	548 (1420)	493
¹ A 62 (57b → 60b); 31 (56b → 60b)	2.65 (468)	0.006	445 (1200)	429
¹ A 97 (59a → 63a);	2.89 (429)	0.004	410 (2240)	388
¹ B 70 (56b → 63a); 26 (57b → 63a)	2.97 (417)	0.012	374 (3000)	362
¹ A 53 (60a → 63a); 15 (57b → 60b); 10 (56b → 60b); 7 (57b → 59b);	3.08 (402)	0.130	307 (14000)	306/297

^[a] Experimental values from spectral deconvolution. Extinction coefficients, ϵ , in M⁻¹·cm⁻¹.

Table 6. Selected calculated lowest TD DFT singlet excitation energies for [(bpy)Ni(Me)₂]

Main character (%)	ADF/SAOP		G03/B3LYP		Experiment	
	Trans. energy in eV (nm)	Osc. strength	Trans. energy in eV (nm)	Osc. strength	λ (nm) in toluene (ϵ) ^[a]	λ (nm) in DMF ^[a]
¹ B ₂ 99 (5a ₂ → 6b ₁);	1.63 (760)	0.006	1.64 (756)	0.002	785 (380)	760
¹ A ₁ 72 (7b ₁ → 8b ₁); 17 (7b ₁ → 9b ₁); 10 (5a ₂ → 6a ₂)	1.87 (663)	0.017	2.24 (553)	0.048	678 (4110)	618
¹ B ₂ 97 (5a ₂ → 9b ₁); 2 (7b ₁ → 6a ₂)	2.02 (614)	0.006	2.75 (451)	0.008	631(3300)	581
¹ B ₂ 96 (7b ₁ → 6a ₂); 2 (5a ₂ → 9b ₁);	2.56 (484)	0.026	3.08 (402)	0.029	461 (2830)	434
¹ A ₁ 48 (5a ₂ → 6a ₂); 24 (7b ₁ → 8b ₁); 24 (7b ₁ → 9b ₁)	2.78 (446)	0.125	3.34 (371)	0.119	416 (4280)	392

^[a] Experimental values from spectral deconvolution. Extinction coefficients, ϵ , in M⁻¹·cm⁻¹.

produce the experimentally obtained bond lengths and angles well. The biggest difference between the two methods was observed for the Ni–C bond, where ADF/BP gave a value of 1.930 Å and G03/B3LYP yielded 1.906 Å for the dimethyl complex compared to the experimental value of 1.923(4) Å.^[30] Approximately the same was found

for the dimesityl derivative. For the bromomesityl complex ADF/BP also gave a far more accurate Ni–Br distance (2.324 Å) compared with the experimental value of 2.300(1) Å (G03/BLYP gave 2.399 Å). Comparing the experimental data of the dimethyl derivative [(bpy)Ni(Me)₂] (monoclinic *P*2₁/*c*, *Z* = 4)^[30] with all the so far structurally characterised

Table 7. Selected calculated lowest TD DFT singlet excitation energies for [(bpy)Ni(Mes)Br]

Main character (%)	ADF/SAOP		G03/B3LYP		Experiment	
	Trans. energy in eV (nm)	Osc. strength	Trans. energy in eV (nm)	Osc. strength	λ (nm) in toluene (ϵ) ^[a]	λ (nm) in DMF ^[a]
¹ A 48 (104a \rightarrow 106a); 30 (103a \rightarrow 106a)	1.64 (756)	0.015	1.82 (682)	0.001	675 (80)	–
¹ A 89 (102a \rightarrow 106a); 6 (104a \rightarrow 106a)	1.69 (734)	0.004	1.85 (669)	0.001	613 (270)	555
¹ A 83 (100a \rightarrow 106a); 5 (104a \rightarrow 107a)	2.13 (582)	0.022	2.04 (607)	0.025	558 (1420)	522
¹ A 52 (103a \rightarrow 107a); 36 (104a \rightarrow 107a)	2.31 (537)	0.005	2.29 (540)	0.001	539 (50)	496
¹ A 43 (104a \rightarrow 108a); 31 (103a \rightarrow 108a); 20 (99a \rightarrow 106a);	2.56 (484)	0.013	2.46 (502)	0.012	512 (2710)	473
¹ A 36 (100a \rightarrow 107a); 36 (99a \rightarrow 106a)	2.71 (457)	0.010	2.60 (476)	0.040	477 (1830)	447
¹ A 53 (100a \rightarrow 107a); 15 (99a \rightarrow 106a)	2.82 (440)	0.025	2.72 (456)	0.004	449 (960)	427
¹ A 68 (105a \rightarrow 109a); 10 (103a \rightarrow 109a)	2.89 (429)	0.010	–	–	418 (900)	–
¹ A 70 (100a \rightarrow 108a); 10 (99a \rightarrow 107a)	3.14 (395)	0.038	3.01 (412)	0.009	380 (1430)	349
¹ A 34 (103a \rightarrow 109a); 30 (102a \rightarrow 109a); 18 (99a \rightarrow 107a); 8 (104a \rightarrow 109a)	3.44 (360)	0.030	–	–	340 (2740)	325

^[a] Experimental values from spectral deconvolution. Extinction coefficients, ϵ , in $\text{M}^{-1}\cdot\text{cm}^{-1}$.

mesitylnickel complexes reveals markedly shorter Ni–C bonds for the latter. This is in contrast to what would be expected on steric grounds. The C–Ni–C angles in the dimesityl derivatives are slightly enlarged to more than 90° (86.6° for the dimethyl derivative). The N–Ni–N chelate bite and the Ni–N bonds, however, do not differ. As a consequence, it seems that in [(bpy)Ni(Me)₂] the inter-ring distance between the pyridine rings is elongated (1.485 Å) which normally means reduced back-bonding. ADF/BP gives a value of 74.4° for the N1–Ni–C11–C12 tilt angle of the mesityl co-ligands (74.9° by G03/B3LYP) and we feel that from these structural data there is already evidence for a notable co-ligand (Mes) contribution to the electronic transitions. The Mes co-ligand therein could act either as a π -donor or π -acceptor. Furthermore, from the EXAFS measurements we have evidence of a strong π -donating interaction of the bromine co-ligand with the nickel atom. Both types of co-ligand contributions will be substantiated by a view of the calculated frontier orbitals. The ground-state one-electron energies and percentage composition of selected highest occupied and lowest unoccupied molecular orbitals have been calculated by DFT methods and the results are shown qualitatively in Figure 6.

The labelling and relative position of ADF/SAOP calculated frontier molecular orbitals is depicted in Figure 6. The calculated composition is available in the Supporting Information. The figure illustrates how the replacement of Mes by other co-ligands influences the composition of the frontier MOs. The character of the LUMO is only moderately influenced by the variation of the co-ligand R.

More substantial changes are observed in the composition of the set of HOMOs which, in the case of [(bpy)Ni(Mes)₂] (**3c**), have large contributions of the Mes co-ligand. This is different for [(bpy)Ni(Me)₂], where the lower lying occupied orbitals are formed by Me sp³ orbitals interacting with central metal orbitals. Both ADF/BP and DFT/B3LYP give qualitatively the same composition for the HOMO and LUMO of [(bpy)Ni(Me)₂], and the composition of the other frontier orbitals does not differ substan-

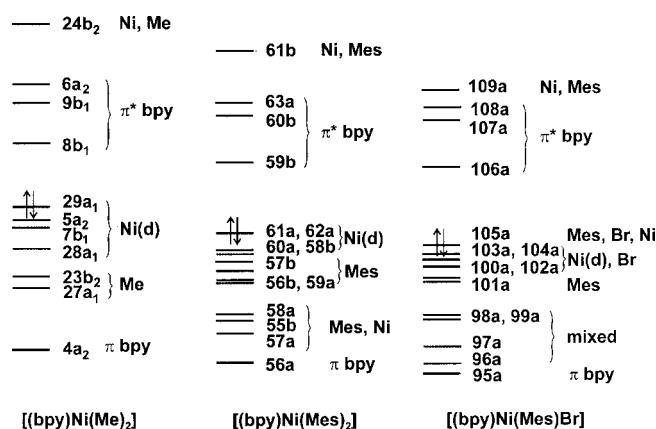


Figure 6. Qualitative MO schemes [(bpy)Ni(Me)₂], [(bpy)Ni(Mes)₂] (**3c**) and [(bpy)Ni(Mes)Br] (**2c**) based on ADF/SAOP calculated one-electron energies and percentage composition of selected frontier molecular orbitals

tially either. In the case of [(bpy)Ni(Mes)Br] (**2c**) bromine p orbitals contribute to a large extent to the HOMOs whereas the contributions of the mesityl co-ligands are lower than for the dimesityl derivative.

To gain insight to the electronic transitions, lowest TD DFT singlet excitation energies have been calculated and compared to experimentally observed absorption maxima. The results are summarised in Tables 5–7. To this end the absorption spectra of the three compounds have been submitted to a spectral deconvolution, as shown in Figure 5. However, the results of the deconvolutions were not unambiguous since both multiple electronic transitions and vibrational progression could contribute to the various maxima observed as shoulders in the spectra.

All calculated transitions have mixed character. They can be characterised as MLCT excitations for [(bpy)Ni(Me)₂], whereas for [(bpy)Ni(Mes)₂] (**3c**) and [(bpy)Ni(Mes)Br] (**2c**) the contribution from the Mes or Br co-ligands cannot be neglected and the corresponding transitions should be assigned as mixtures of MLCT/L'LCT [ligand (Mes)-to-li-

gand charge transfer] or MLCT/XLCT (halogen-to-ligand charge transfer), respectively. Both co-ligands thus act as π -donors. In the bromomesityl complex the donor character of the mesityl group is lower than the dimesityl derivative. The transition energies agree qualitatively quite well with experimental ones for the dimesityl and dimethyl derivatives (Table 5 and 6). Note that the solvatochromic effects are enormous for most absorption bands. Generally, G03/B3LYP predicts larger transition energies than ADF/SAOP, as shown in Table 7. For **2c** the ADF/SAOP calculations predict very low-energy transitions around 1.64 eV (750 nm), which cannot be found in the absorption spectra; the TD-DFT method using "pure" functionals underestimates the transitions energies also in the case of other halide complexes.^[31] The transitions calculated at higher energies fit better to experimentally found ones; however the intensity pattern is not reproduced well. G03 calculations using hybrid B3LYP functionals give transitions with high bromine contributions closer to the experimentally measured weak, low-lying absorption bands.

Resonance Raman Spectroscopy

In many cases the character of the excited states of transition metal complexes has been studied by emission spectroscopy.^[32] However, of the present nickel complexes only **2a**, **2b**, **2h** and **3a** show very weak emission in the solid or solution; the others do not emit either in the solid or in solution, even at 110 K. Additionally, for the weakly emitting compounds the obtained results are ambiguous. We therefore embarked on a combination of resonance Raman (rR) spectroscopy and quantum chemical calculations to probe the character of the excited states. The rR technique allows us to draw direct conclusions about the character of the electronic transitions since it is based on the presumption that only those Raman bands due to vibrations that are influenced by the electronic transition that is excited are enhanced in intensity.^[33] The rR spectra of the dimesityl complexes and selected bromomesityl complexes dispersed in KNO_3 were recorded after irradiation of their lowest-energy absorption bands; examples are displayed in Figure 7. Selected data are collected in Table 8 (see also Supporting Information) in comparison to DFT calculated Raman active vibrations for the model system $[(\text{bpy})\text{Ni}(\text{Me})_2]$ and the resonances of free bpy.^[34]

Based on these calculations and data the resonances observed for $[(\text{bpy})\text{Ni}(\text{Mes})_2]$ (**3c**) at 1608, 1561, 1485, 1322, 1277, 1167, 1015, 655 and 370 cm^{-1} can be assigned to the normal modes of the bpy ligand. They have been observed previously in rR experiments with a number of bpy complexes upon excitation into their metal-to-ligand(bpy) charge-transfer bands.^[35] The resonance at highest energy is assigned to the $\nu(\text{C}=\text{N})$ vibration. Its energy decreases along the series $\text{tmphen} > \text{bpy} > \text{bpz}$ which is caused by the increasing π -accepting abilities from tmphen to bpz. Resonances at 426, 343 and 241 cm^{-1} were assigned to the metal-ligand modes $\nu(\text{Ni}-\text{C})$, $\nu(\text{Ni}-\text{N})$ and $\delta(\text{Ni}-\text{N})$,

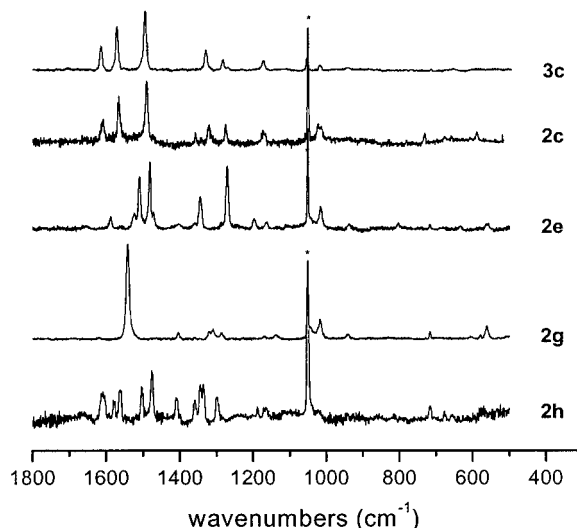


Figure 7. Resonance Raman spectra of the nickel complexes $[(\text{bpy})\text{Ni}(\text{Mes})_2]$ (**3c**; $\lambda_{\text{ex}} = 542\text{ nm}$), $[(\text{bpy})\text{Ni}(\text{Mes})\text{Br}]$ (**2c**; $\lambda_{\text{ex}} = 488\text{ nm}$), $[(\text{bpz})\text{Ni}(\text{Mes})\text{Br}]$ (**2e**; $\lambda_{\text{ex}} = 592\text{ nm}$), $[(i\text{Pr-DAB})\text{Ni}(\text{Mes})\text{Br}]$ (**2g**; $\lambda_{\text{ex}} = 598\text{ nm}$) and $[(\text{terpy})\text{Ni}(\text{Mes})\text{Br}]$ (**2h**; $\lambda_{\text{ex}} = 457.9\text{ nm}$), obtained from KNO_3 pellets upon irradiation into the long-wavelength absorption bands; * denotes the 1051 cm^{-1} resonance of NO_3^- .

respectively. For the other diimine ligands the assignment is based on comparison with the bpy analogue.

At first sight (e.g. in Figure 7 for the two bpy complexes) the rR spectra of the bromomesityl complexes of the aromatic diimine ligands are much the same as those recorded for the dimesityl complexes. For the *i*Pr-DAB complex assignment of the observed resonances at 1542 cm^{-1} $\nu(\text{C}=\text{N})$, or 1170, 1138 and 1020 cm^{-1} $\nu(\text{C}-\text{C})$ was facilitated by comparison with recently examined organoplatinum(II) and -platinum(IV) complexes.^[29b,36] A closer look at the data reveals that in the dimesityl complexes some resonances are observed that do not appear for the bromomesityl derivatives, for example for bpy: 1263, 1114 and 941 and 740 cm^{-1} (marked in italics in Table 8). Such resonances are characteristic of $\nu(\text{C}=\text{C}_{\text{ring}})$ or δ_{ring} vibrations and could be assigned to the mesityl co-ligands. They appear only for the dimesityl complexes because the contribution of the mesityl co-ligands to the excited state is markedly higher (mixed MLCT/L/LCT) than for the bromomesityl complexes (mixed XLCT/MLCT) thus supporting the results from quantum chemical calculation (vide supra). The mentioned resonances might also be interpreted as bpy-centred resonances and their occurrence explained by the differences in symmetry between dimesityl (C_2) and bromomesityl (C_s). However, it is unlikely that the higher-symmetry molecules exhibit more resonances than the lower-symmetry ones.

Support for the partial XLCT character of the excited states in the bromomesityl complexes could not be obtained from rR spectra. The only relevant vibration, $\nu(\text{Ni}-\text{Br})$, which occurs around $160\text{--}170\text{ cm}^{-1}$, is quite weak and therefore hard to detect in the rR experiment due to the closeness to the excitation line. Furthermore, it is also possible that the Ni-Br σ -bond is not much distorted upon π -

Table 8. Selected resonance Raman data of [(bpy)Ni(Mes)₂] (**3c**), [(bpy)Ni(Mes)Br] (**2c**) and [(terpy)Ni(Mes)]Br (**2h**) compared to calculated [(bpy)Ni(Mes)₂] and the free ligand^[a]

λ_{ex}	3c $\tilde{\nu}$ (cm ⁻¹) 542 nm	2c $\tilde{\nu}$ (cm ⁻¹) 488 nm	2h $\tilde{\nu}$ (cm ⁻¹) 457.9 nm	Calculated ^[b] $\tilde{\nu}$ (cm ⁻¹)	bpy ^[c] $\tilde{\nu}$ (cm ⁻¹)	Assignment
1	1608	1603	1608	1590	1579	$\nu(\text{C}=\text{C}_{\text{ring}}) + \nu(\text{C}=\text{N}_{\text{ring}})$
2	1561	1565	1577/1561	1549	1553	$\nu(\text{C}=\text{C}_{\text{ring}}) + \nu(\text{C}=\text{N}_{\text{ring}})$
3	1485	1490	1503/1475	1463	1448	$\nu(\text{C}=\text{C}_{\text{ring}})/\delta(\text{H})$
4	— ^[c]	— ^[c]	1408	1414	1401	$\nu(\text{C}=\text{C}_{\text{ring}})/\delta(\text{H})$
5	1322	1325	1336	1296	1270	$\nu(\text{C}-\text{C}_{\text{interring}})$
6	1277	1280	1299	1273	1248	$\nu(\text{C}=\text{N}_{\text{ring}}) + \nu(\text{C}=\text{C}_{\text{ring}})$
7	<i>1263</i>	— ^[c]	— ^[c]	—	—	$\nu(\text{C}=\text{C}_{\text{ring}})$
8	1167	1177	1172	1152	1210	$\delta(\text{H})/\nu(\text{C}=\text{C}_{\text{ring}})$
9	<i>1114</i>	— ^[c]	— ^[c]	—	1138	$\delta(\text{H})/\nu(\text{C}=\text{C}_{\text{ring}})$
10	1015	1020	1023	1047	1090	$\delta(\text{H})/\text{ring breathe}$
11	<i>941</i>	— ^[c]	— ^[c]	—	—	$\delta(\text{ring})$
12	<i>740</i>	— ^[c]	— ^[c]	—	—	$\delta(\text{ring})$
13	655	770	676	643	651	$\delta(\text{ring bend})$
14	565	650	654	542	618	$\nu(\text{Ni}-\text{C})$
15	426	564	557	421	—	$\delta(\text{N}-\text{Ni}-\text{N})_{\text{out-of-plane}}$
16	370	376	n.m.	383	398	$\nu(\text{Ni}-\text{N}) + \delta(\text{C}-\text{Ni}-\text{C})$
17	343	n.m.	n.m.	358	—	$\nu(\text{Ni}-\text{N})$
18	241	n.m.	n.m.	224	—	$\delta(\text{N}-\text{Ni}-\text{N})$

^[a] From resonance Raman experiments on KNO₃ pellets at ambient temperature. Excitation wavelengths, λ_{ex} , coincident with the long-wavelength absorption maximum. ^[b] Calculated for [(bpy)Ni(Mes)₂] by G03/B3LYP; scaling factor 0.9613.^[37] ^[c] Not observed. n.m. = not measured; resonances of **3c** marked in *italics* are assigned to mesityl vibrations (see text).

donation by the bromine atom and therefore not resonantly enhanced.

Conclusion

Quantum chemical calculations have revealed the interplay of the metal centre, the chelating diimine ligand and the co-ligands methyl, mesityl or bromine to form the frontier orbitals relevant for the optical transitions and excited states. Strong experimental evidence for the π -accepting mode of the chelate ligand and the π -donating modes of the mesityl and bromine co-ligands comes from a combination of spectroscopic methods. A structural study using EXAFS spectroscopy shows some clear trends for the metal–ligand distances that can be explained by varying σ -donor and/or π -acceptor ability through the series of diimine ligands and π -donating contributions from the bromine co-ligand. Support for a specific electronic contribution from the mesityl co-ligand comes from XRD results. The absorption spectra agree qualitatively well with the calculated transitions. Resonance Raman spectroscopy strongly supports the π -accepting character of the diimine ligands. The evidence for the co-ligand contributions is less strong and should be further substantiated by rR studies on structurally varied derivatives (H/D exchange, other aryl co-ligands, Cl/Br/I exchange). Such studies are already underway.

Experimental Section

Instrumentation: ¹H NMR spectra were recorded on Bruker AC250 or AM200 spectrometers. UV/Vis absorption spectra were recorded

on Bruins Instruments Omega 10, Hewlett–Packard 8453 Diode Array and Varian Cary 4E spectrophotometers. Resonance Raman spectra of the complexes dispersed in KNO₃ pellets were recorded on a Dilor XY spectrometer equipped with a Wright Instruments CCD detector, using a Spectra Physics 2040E Ar⁺ and Coherent CR490 and CR590 dye lasers (with Coumarin 6 and Rhodamine 6G dyes) as excitation sources. Emission spectra were recorded on a Perkin–Elmer LS5B spectrophotometer.

Computational Details: Ground-state electronic structure calculations on complexes [(bpy)Ni(R)₂] and [(bpy)Ni(Mes)Br] (**2c**) have been done on the base of density-functional theory (DFT) methods using the ADF2002.03^[38] and Gaussian 03^[39] program packages. The lowest excited states of the closed-shell complexes were calculated by the time-dependent DFT (TD DFT) method (both ADF and G03 programs).

Within the ADF program, Slater-type orbital (STO) basis sets of triple- ζ quality with polarisation functions were employed; methyl groups on the Mes co-ligands were described by basis sets of double- ζ quality with polarisation functions. The inner shells were represented by a frozen core approximation (1s for C, N, 1s-3p for Br and 1s-3p for Ni were kept frozen). The following density functionals were used within ADF: the local density approximation (LDA) with VWN parametrisation of electron gas data or the functional including Becke's gradient correction^[40] to the local-exchange expression in conjunction with Perdew's gradient correction^[41] to the LDA expression (ADF/BP). The scalar relativistic (SR) zero-order regular approximation (ZORA) was used within this study. Compositions and energies of molecular orbitals and electronic transition energies and compositions were calculated by the asymptotically correct SAOP functional,^[42] which is suitable also for higher-lying MOs and electronic transitions. Core electrons were included in ADF/SAOP calculations.

Within Gaussian 03 6-31G* polarized double- ζ basis sets^[43] for C, N, H and Ni atoms; effective core pseudopotentials with corresponding optimised set of basis functions for Br atom^[44] were used

for geometry optimisation and frequency calculations. Correlation consistent polarized double- ζ basis sets^[45] (cc-pVDZ) within TD-DFT calculations. Hybrid Becke's three parameter functional with Lee, Yang and Parr correlation functional (B3LYP)^[46] was used in Gaussian 03 calculations (G03/B3LYP). Gaussian 03 was also used for the calculations of the vibrations at G03/B3LYP optimised geometries.

The calculations on [(bpy)Ni(Me)₂] and [(bpy)Ni(Mes)₂] (**3c**) were performed in a C_{2v} or C₂ constrained symmetry, respectively. The *z* axis is coincident with the C₂ symmetry axis; the central atom and bpy ligand lie in the *y,z* plane. All results discussed correspond to optimised geometries. The calculations on [(bpy)Ni(Mes)Br] were done without any symmetry constrains.

Crystal Structure Analysis for [(tmphen)Ni(Mes)₂] (3a**):** Data collection was performed at *T* = 173(2) K on a Siemens P4 diffractometer with Mo-*K*_α radiation (λ = 0.71073 Å). The structure was solved by direct methods using the SHELXTL-PLUS package^[47] and refinement was carried out with SHELXL-97 employing full-matrix least-squares methods on *F*² with *F*_o² = 3σ(*F*_o²). Formula (*M*_w) C₃₄H₃₈N₂Ni₁ (533.37); cell dimensions (Å): *a* = 16.297(3), *b* = 16.578(3), *c* = 20.732(4); *V* = 5601.3(19) Å³; *Z* = 8; Abs. coefficient = 0.718 mm⁻¹; *F*(000) = 2272; GooF at *F*² = 1.174; *R* values [*I* > 2σ(*I*): *R*1 = 0.0801, *wR*2 = 0.1679; *R* values (all data): *R*1 = 0.164, *wR*2 = 0.2076; max./min. 0.609/−0.508 e·Å⁻³. Empirical absorption correction was performed using Ψ-scans. All non-hydrogen atoms were treated anisotropically, hydrogen atoms were included by using appropriate riding models. CCDC-226909 (for **3a**) contains the supplementary crystallographic data for this paper. These data can be obtained free of charge at www.ccdc.cam.ac.uk/conts/retrieving.html [or from the Cambridge Crystallographic Data Centre, 12 Union Road, Cambridge CB2 1EZ, UK; Fax: +44-1223-336-033; E-mail: deposit@ccdc.cam.ac.uk].

EXAFS Measurements: The XANES and EXAFS measurements were performed at the beamlines X1.1 (RÖMO II) and E4 at the Hamburger Synchrotronstrahlungslabor des Deutschen Elektronensynchrotrons (HASYLAB at DESY, Hamburg, Germany), at beamline 2–3 at the Stanford Synchrotron Radiation Laboratory (SSRL) at SLAC (Stanford, USA) or at the newly designed EXAFS-beamline KMC-2 at the Berliner Elektronenspeicherring-Gesellschaft für Synchrotronstrahlung m.b.H (BESSY II, Berlin, Germany).

For the measurements at the Ni-K edge (8332.8 eV) a Si(111) double crystal monochromator was used at the SSRL and at DESY. For the measurements at the Br-K edge (13474.0 eV) at beamline X1.1 a Si(311) double crystal monochromator was used. At BESSY a SiGe(220) double graded-crystal (0.5% Ge/cm) monochromator was used for the nickel and the bromine edge. The synchrotron beam current was between 80 and 100 mA at HASYLAB (positron energy 4.45 GeV), between 100 and 250 mA at BESSY (electron energy 1.7 GeV) and between 80 and 100 mA at the SSRL (electron energy 1.7 GeV).

All the experiments were carried out under ambient conditions at 25 °C. The tilt of the second monochromator crystal was set to 30% harmonic rejection. Energy resolution was estimated to be about 0.7–2.0 eV for the Ni-K edge and 4.0 eV for the Br-K edge. The spectra were collected in transmission mode with ion chambers. All ion chambers were filled with nitrogen in the case of the measurements at the Ni-K edge, and the second and third chamber with argon in the case of the measurements at the Br-K edge. Energy calibration was performed with nickel metal foil in the case of measurements at the Ni-K edge and lead metal foil (Pb L_{III}-edge)

in the case of the Br-K edge. The solid complexes were embedded in a polyethylene matrix and pressed to pellets. The concentration of all samples was adjusted to yield an absorption jump, $\Delta\mu$, of about 1.5.

Data evaluation started with background absorption removal from the experimental absorption spectrum by subtraction of a Victoreen-type polynomial. Then, the background-subtracted spectrum was convoluted with a series of increasingly broader Gauss functions and the common intersection point of the convoluted spectra was taken as energy *E*₀.^[48] To determine the smooth part of the spectrum, corrected for pre-edge absorption, a piecewise polynomial was used. It was adjusted in such a way that the low-*R* components of the resulting Fourier transform were minimal. After division of the background-subtracted spectrum by its smooth part, the photon energy was converted into photoelectron wavenumbers *k*. The resulting EXAFS function was weighted with *k*³. Data analysis in *k*-space was performed according to the curved wave multiple scattering formalism of the program EXCURV92 with XALPHA phase and amplitude functions.^[49] The mean-free path of the scattered electrons was calculated from the imaginary part of the potential (VPI was set to −4.00) and an overall energy shift (ΔE_0) was assumed. The Amplitude Reduction Factor (AFAC) was set to a value of 0.8 in the case of the Ni-K as well as the Br-K edge.

Materials and Procedures: The precursor complex [(PPh₃)₂Ni(Mes)Br] (**1**)^[23] and the ligands bpm,^[50] bpz,^[51] and *i*Pr-DAB^[52] were obtained following literature procedures. Mesityllithium was prepared according to the method of Biali et al.^[53] Other reagents were commercially available and used without further purification. All preparations and physical measurements were carried out in dried solvents under an argon atmosphere, using Schlenk techniques.

Preparation of [(N[^]N)Ni(Mes)Br] (2**) [N[^]N = tmphen (a), dmbpy (b), bpy (c), bpym (d), bpz (e) bpm (f), and terpy (h)]:** In a typical reaction 2 g of [(PPh₃)₂Ni(Mes)Br] (**1**) (2.56 mmol) were suspended in 250 mL of toluene, 1.1 equivalents of the ligand was added and the solution stirred overnight at ambient temperature. The reaction volume was then reduced to 20 mL and the resulting solids were filtered off. They were washed with small amounts of toluene (2 × 5 mL) and *n*-pentane (3 × 20 mL) and dried. For bpz and bpm the products were recrystallised twice from a mixture of CH₂Cl₂ and *n*-heptane (1:8). From the filtrates only small amounts of clean products could be isolated after evaporation to dryness and recrystallisation from CH₂Cl₂/*n*-heptane (1:8). For analytical data see Table 1 and Supporting Information.

Preparation of Bromo-1,4-diisopropyl-1,4-diazabutadienemesitylnickel(II), [(*i*Pr-DAB)Ni(Mes)Br] (2g**):** *i*Pr-DAB (250 mg, 1.78 mmol) was added to a vigorously stirred suspension of [(PPh₃)₂Ni(Mes)Br] (**1**; 250 mg, 0.32 mmol) in 500 mL of *n*-pentane. After a few minutes the yellow suspension dissolved leaving a violet voluminous precipitate that was finally filtered off. The obtained violet solid was recrystallised from CH₂Cl₂/*n*-heptane (1:8) and dried, yielding 112 mg of dark-violet microcrystalline material. For analytical data see Table 1 and Supporting Information.

Preparation of the Dimesitylnickel Complexes **3a, **3c**, **3e**:** The dimesitylnickel complexes [(N[^]N)Ni(Mes)₂] were prepared as described for the bpy complex^[23] from the bromomesityl complexes and mesityllithium.

3a: Yield 88%, dark violet powder. C₃₄H₃₈N₂Ni₁ (533.40); calcd. C 76.56, H 7.18, N 5.25; found C 76.59, H 7.23, N 5.27. ¹H NMR ([D₆]DMSO): δ = 8.26 (s, 2 H, H5,6), 7.64 (s, 2 H, H2,9), 6.45 (s, 4 H, *m*-H), 2.67 (s, 6 H, H₃C^{4,7}), 2.64 (s, 12 H, *o*-CH₃), 2.29 (s, 6

H, H₃C^{3,8}), 2.13 (s, 6 H, *p*-CH₃) ppm. ¹³C NMR (CD₂Cl₂): δ = 157.2, 150.5, 142.6, 127.3, 122.7 (all tmphen); 144.9 (Mes-1), 144.1 (Mes-2), 130.9 (Mes-4), 125.3 (Mes-3), 27.3 (*o*-CH₃), 20.8 (*p*-CH₃), 18.1 (H₃C^{4,7}), 14.9 (H₃C^{3,8}) ppm.

3c: Yield 84%, dark violet powder. C₂₈H₃₀N₂Ni₁ (453.27): calcd. C 74.20, H 6.67, N 6.18; found C 74.35, H 6.65, N 6.22. ¹H NMR ([D₆]acetone): δ = 8.38 (d, ³J_{H3,H4} = 8.02 Hz, 2 H, H3,3'), 8.12 (dd, ³J_{H4,H5} = 6.90 Hz, 2 H, H4,4), 7.54 (d, ³J_{H5,H6} = 4.84 Hz, 2 H, H6,6'), 7.44 (dd, 2 H, H5,5'), 6.37 (s, 4 H, *m*-H), 2.53 (s, 12 H, *o*-CH₃), 2.08 (s, 6 H, *p*-CH₃) ppm. ¹³C NMR ([D₆]acetone): δ = 157.4 (bpy-2,2'), 149.9 (bpy-6,6'), 144.1 (Mes-2), 138.1 (bpy-4,4'), 136.6 (Mes-1), 130.9 (Mes-4), 127.6 (bpy-3,3'), 126.0 (Mes-3), 122.0 (bpy-5,5'), 27.3 (*o*-CH₃), 20.8 (*p*-CH₃) ppm.

3e: Yield 78%, dark green microcrystalline powder. C₂₆H₂₈N₄Ni₁ (455.25): calcd. C 68.60, H 6.20, N 12.31; found C 68.72, H 6.22, N 12.41. ¹H NMR ([D₆]acetone): δ = 9.54 (s, 2 H, H3,3'), 8.75 (s, 2 H, H5,5'), 7.53 (s, 2 H, H6,6'), 6.49 (s, 4 H, *m*-H), 2.45 (s, 12 H, *o*-CH₃), 2.28 (s, 6 H, *p*-CH₃) ppm.

Supporting Information: Fourteen tables with comparisons between calculated and experimental structural data for **2c**, **3c**, and [(bpy)-Ni(Me)₂]; details of the crystal structure of **3a**; ¹³C NMR spectroscopic data of selected complexes and absorption spectroscopic data are also given. Furthermore, eight figures are provided showing additional EXAFS spectra and the XANES spectra of **2e** and **2d** and a view of the unit cell of **3a** from the crystal structure determination (see also the footnote on the first page of this article).

Acknowledgments

We wish to thank HASYLAB at DESY (Hamburg, Germany), the SSRL at SLAC (Stanford, USA) and BESSY (Berlin, Germany) for providing synchrotron radiation. The SSRL is operated by the U.S. Department of Energy, Office of Basic Energy Science. Ministry of Education of the Czech Republic and the COST Action D14 is gratefully acknowledged.

- [1] [1a] S. D. Ittel, L. K. Johnson, M. Brookhart, *Chem. Rev.* **2000**, *100*, 1169. [1b] C. M. Killian, L. K. Johnson, M. Brookhart, *Organometallics* **1997**, *16*, 2005. [1c] S. Mecking, L. K. Johnson, L. Wang, M. Brookhart, *J. Am. Chem. Soc.* **1998**, *120*, 888. [1d] A. M. LaPointe, M. Brookhart, *Organometallics* **1998**, *17*, 1530.
- [2] A. Michalak, T. Ziegler, *Organometallics* **2001**, *20*, 1521.
- [3] [3a] S. Mecking, *Angew. Chem.* **2001**, *113*, 550; *Angew. Chem. Int. Ed.* **2001**, *40*, 534. [3b] A. Held, S. Mecking, *Chem. Eur. J.* **2000**, *6*, 4623.
- [4] G. J. P. Britovsek, V. C. Gibson, D. F. Wass, *Angew. Chem.* **1999**, *111*, 448; *Angew. Chem. Int. Ed.* **1999**, *38*, 428.
- [5] M. Schmid, R. Eberhardt, M. Klinga, M. Leskelä, B. Rieger, *Organometallics* **2001**, *20*, 2321.
- [6] J. Heinicke, M. He, A. Dal, H.-F. Klein, O. Hetche, W. Keim, U. Flörke, H.-J. Haupt, *Eur. J. Inorg. Chem.* **2000**, *3*, 431.
- [7] C. Wang, S. Friedrich, T. R. Younkin, R. T. Li, R. H. Grubbs, D. A. Bansleben, M. W. Day, *Organometallics* **1998**, *17*, 3149.
- [8] M. Schmid, R. Eberhardt, J. Kukral, B. Rieger, *Z. Naturforsch., Teil B* **2002**, *57*, 1141.
- [9] L. Johnson, L. Wang, S. McLain, A. Bennett, K. Dobbs, E. Hauptman, A. Ionkin, S. Ittel, K. Kunitsky, W. Marshall, E. McCord, C. Radzewich, A. Rinehart, K. J. Sweetman, Y. Wang, Z. Yin, M. Brookhart, *ACS Symp. Ser.* **2003**, *857*, 131.
- [10] [10a] J. L. Davis, B. A. Arndtsen, *Organometallics* **2000**, *19*, 4657. [10b] C. Geyer, S. Schindler, *Organometallics* **1998**, *17*, 4400.
- [11] P. T. Matsunaga, J. C. Mavrapoulos, G. L. Hillhouse, *Polyhedron* **1995**, *14*, 175.
- [12] P. T. Matsunaga, C. R. Hess, G. L. Hillhouse, *J. Am. Chem. Soc.* **1994**, *116*, 3665.
- [13] P. T. Matsunaga, G. L. Hillhouse, *J. Am. Chem. Soc.* **1993**, *115*, 2075.
- [14] P. Binger, M. J. Doyle, C. Krüger, Y.-H. Tsay, *Z. Naturforsch., Teil B* **1979**, *34*, 1289.
- [15] T. Yamamoto, A. Yamamoto, S. Ikeda, *J. Am. Chem. Soc.* **1971**, *93*, 3350.
- [16] W. Seidel, *Z. Chem.* **1985**, *25*, 411.
- [17] G. Wilke, G. Herrmann, *Angew. Chem.* **1966**, *78*, 591. G. Wilke, G. Herrmann, *Angew. Chem. Int. Ed. Engl.* **1966**, *5*, 581.
- [18] T. R. Miller, I. G. Dance, *J. Am. Chem. Soc.* **1973**, *95*, 6970.
- [19] A. Arcas, P. Royo, *Inorg. Chim. Acta* **1978**, *31*, 97.
- [20] R. F. de Souza, L. C. Simon, M. C. Alves, *J. Catal.* **2003**, *214*, 165.
- [21] T. Yamamoto, M. Abla, Y. Murakami, *Bull. Chem. Soc. Jpn.* **2002**, *75*, 1997.
- [22] [22a] T. Yamamoto, M. Abla, *J. Organomet. Chem.* **1997**, *535*, 209. [22b] T. Yamamoto, *Synlett* **2003**, *4*, 425. [22c] T. Yamamoto, S. Wakabayashi, K. Osakada, *J. Organomet. Chem.* **1992**, *428*, 223.
- [23] A. Klein, *Z. Anorg. Allg. Chem.* **2001**, *627*, 645.
- [24] M. P. Feth, A. Klein, H. Bertagnolli, *Eur. J. Inorg. Chem.* **2003**, 839.
- [25] [25a] A. Klein, E. J. L. McInnes, W. Kaim, *J. Chem. Soc., Dalton Trans.* **2002**, 2371. [25b] A. Klein, H.-D. Hausen, W. Kaim, *J. Organomet. Chem.* **1992**, *440*, 207. [25c] A. Klein, M. Niemeyer, *Z. Anorg. Allg. Chem.* **2000**, *626*, 1191. [25d] A. Klein, J. van Slageren, S. Zális, *Eur. J. Inorg. Chem.* **2003**, 1927.
- [26] [26a] G. J. Colpas, M. J. Maroney, C. Bagyinka, M. Kumar, W. S. Willis, S. L. Suib, N. Baidya, P. K. Mascharak, *Inorg. Chem.* **1991**, *30*, 920. [26b] M. W. Renner, L. R. Furenlid, K. M. Barkigia, J. Fajer, *J. Phys. IV France* **1997**, *7*, 661. [26c] N. Kosugi, T. Yokoyama, K. Asakura, H. Kuroda, *Chem. Phys.* **1984**, *91*, 249. [26d] H. Nishida, T. Yokoyama, H. Kuroda, *Chem. Phys.* **1986**, *104*, 449.
- [27] D. M. Manuta, A. J. Lees, *Inorg. Chem.* **1983**, *22*, 3825.
- [28] W. Kaim, S. Ernst, S. Kohlmann, *Chem. unserer Zeit* **1987**, *21*, 50.
- [29] [29a] A. Klein, J. van Slageren, S. Záliš, *Eur. J. Inorg. Chem.* **2003**, 1917. [29b] A. Klein, J. van Slageren, S. Záliš, *Inorg. Chem.* **2002**, *41*, 5216.
- [30] G. C. Tucci, R. H. Holm, *J. Am. Chem. Soc.* **1995**, *117*, 6489.
- [31] M. Turki, C. Daniel, S. Zalis, A. Vlček, Jr, J. Van Slageren, D. J. Stufkens, *J. Am. Chem. Soc.* **2001**, *123*, 11431.
- [32] [32a] P. C. Ford, in *Inorganic and Organometallic Photochemistry* (Ed.: M. S. Wrighton), ACS, Washington, D.C., **1978**, vol. 168, 73. [32b] A. B. P. Lever, *Inorganic Electronic Spectroscopy*, Elsevier, Amsterdam, **1984**.
- [33] R. J. H. Clark, T. J. Dines, *Angew. Chem.* **1986**, *98*, 131. R. J. H. Clark, T. J. Dines, *Angew. Chem. Int. Ed. Engl.* **1986**, *25*, 131.
- [34] [34a] J. S. Strukl, J. L. Walter, *Spectrochim. Acta* **1971**, *27*, 223. [34b] J. S. Strukl, J. L. Walter, *Spectrochim. Acta* **1971**, *27*, 209.
- [35] [35a] I. Srnova-Sloufova, B. Vlckova, T. L. Snoeck, D. J. Stufkens, P. Matejka, *Inorg. Chem.* **2000**, *39*, 3551. [35b] R. Hage, J. G. Haasnoot, D. J. Stufkens, T. L. Snoeck, J. G. Vos, J. Reedijk, *Inorg. Chem.* **1989**, *28*, 1413. [35c] P. A. Mabrouk, M. S. Wrighton, *Inorg. Chem.* **1986**, *25*, 526. [35d] R. W. Balk, T. L. Snoeck, D. J. Stufkens, A. Oskam, *Inorg. Chem.* **1980**, *19*, 3015.
- [36] [36a] J. van Slageren, D. J. Stufkens, S. Zalis, A. Klein, *J. Chem. Soc., Dalton Trans.* **2002**, 218. [36b] J. van Slageren, A. Klein, S. Zalis, D. J. Stufkens, *Coord. Chem. Rev.* **2001**, *219–221*, 937.
- [37] M. W. Wong, *Chem. Phys. Lett.* **1996**, *256*, 391.
- [38] [38a] C. Fonseca Guerra, J. G. Snijders, G. Te Velde, E. J. Baerends, *Theor. Chim. Acc.* **1998**, *99*, 391. [38b] S. J. A. van Gisbergen, J. G. Snijders, E. J. Baerends, *Comput. Phys. Commun.* **1999**, *118*, 119.

- [39] Gaussian 03, Revision B.2, M. J. Frisch, G. W. Trucks, H. B. Schlegel, G. E. Scuseria, M. A. Robb, J. R. Cheeseman, J. A. Montgomery, Jr., T. Vreven, K. N. Kudin, J. C. Burant, J. M. Millam, S. S. Iyengar, J. Tomasi, V. Barone, B. Mennucci, M. Cossi, G. Scalmani, N. Rega, G. A. Petersson, H. Nakatsuji, M. Hada, M. Ehara, K. Toyota, R. Fukuda, J. Hasegawa, M. Ishida, T. Nakajima, Y. Honda, O. Kitao, H. Nakai, M. Klene, X. Li, J. E. Knox, H. P. Hratchian, J. B. Cross, C. Adamo, J. Jaramillo, R. Gomperts, R. E. Stratmann, O. Yazyev, A. J. Austin, R. Cammi, C. Pomelli, J. W. Ochterski, P. Y. Ayala, K. Morokuma, G. A. Voth, P. Salvador, J. J. Dannenberg, V. G. Zakrzewski, S. Dapprich, A. D. Daniels, M. C. Strain, O. Farkas, D. K. Malick, A. D. Rabuck, K. Raghavachari, J. B. Foresman, J. V. Ortiz, Q. Cui, A. G. Baboul, S. Clifford, J. Cioslowski, B. B. Stefanov, G. Liu, A. Liashenko, P. Piskorz, I. Komaromi, R. L. Martin, D. J. Fox, T. Keith, M. A. Al-Laham, C. Y. Peng, A. Nanayakkara, M. Challacombe, P. M. W. Gill, B. Johnson, W. Chen, M. W. Wong, C. Gonzalez, J. A. Pople, Gaussian, Inc., Pittsburgh PA, **2003**.
- [40] A. D. Becke, *Phys. Rev. A* **1988**, *38*, 3098.
- [41] J. P. Perdew, *Phys. Rev. A* **1986**, *33*, 8822.
- [42] P. R. T. Schipper, O. V. Gritsenko, S. J. A. van Gisbergen, E. J. Baerends, *J. Chem. Phys.* **2000**, *112*, 1344.
- [43] [43a] P. C. Hariharan, J. A. Pople, *Theor. Chim. Acta* **1973**, *28*, 213. [43b] V. A. Rassolov, J. A. Pople, M. A. Ratner, T. L. Windus, *J. Chem. Phys.* **1998**, *109*, 1223.
- [44] A. Bergner, M. Dolg, W. Kuechle, H. Stoll, H. Preuss, *Mol. Phys.* **1993**, *80*, 1431.
- [45] D. E. Woon, T. H. J. Dunning, *J. Chem. Phys.* **1993**, *98*, 1358.
- [46] P. J. Stephens, F. J. Devlin, C. F. Cabalowski, M. J. Frisch, *J. Phys. Chem.* **1994**, *98*, 11623.
- [47] [47a] G. M. Sheldrick, SHELXTL, Bruker Analytical X-ray Systems, Madison, Wisconsin, USA, **1998**. [47b] G. M. Sheldrick, SHELXL-97: A program for Crystal Structure Determination, University of Göttingen, Göttingen, Germany, **1997**.
- [48] [48a] T. S. Ertel, H. Bertagnolli, S. Hückmann, U. Kolb, D. Peter, *Appl. Spectrosc.* **1992**, *46*, 690. [48b] M. Newville, P. Livins, Y. Yakoby, J. J. Rehr, E. A. Stern, *Phys. Rev. B* **1993**, *47*, 14126.
- [49] S. J. Gurman, N. Binsted, I. Ross, *J. Phys. C* **1986**, *19*, 1845.
- [50] F. Effenberger, *Chem. Ber.* **1965**, *98*, 2260.
- [51] J. J. Lafferty, F. H. Case, *J. Org. Chem.* **1967**, *32*, 1591.
- [52] J. M. Kliegman, R. K. Barnes, *Tetrahedron* **1970**, *26*, 2555.
- [53] S. E. Biali, Z. Rappoport, *J. Am. Chem. Soc.* **1985**, *107*, 1007.

Received December 19, 2003

Early View Article

Published Online April 26, 2004